ELG 6373

CURRENT DIRECTIONS FOR III-V MULTI-JUNCTION SOLAR CELL DEVELOPMENT

March 18, 2014

1. Introduction

Over the past ten years, III-V multi-junction solar cells under concentration have consistently shown the highest efficiencies of all solar cell types, with steady increases year-over-year and record efficiencies currently at 44.7% [1, 2]. Concentrating photovoltaic (CPV) systems using multi-junction cells have been demonstrated with system efficiency greater than 30% [1]. The market for such devices is driven by applications where the cost of the solar cell is small compared with the overall cost to deploy the system, and hence relatively complicated or expensive manufacturing techniques may be warranted. In the case of terrestrial CPV systems, whose returns are directly related to energy production and which may have a relatively small profit margin initially, any increase in efficiency (and hence energy production) should significantly increase profitability [3]. In the case of space-based power systems, the cell cost is negligible compared with the launch costs required to put the power system into orbit [4], and any increase in efficiency will reduce the size and weight of the solar array and its supporting structure and will justify increased costs.

At present, the dominant commercial multi-junction cell design is a lattice-matched structure of $Ga_{0.51}In_{0.49}P$, GaAs and Ge sub-cells on a germanium substrate; the bottom, Ge sub-cell is formed by diffusion of As atoms during the initial growth of III-V material on the Ge substrate, while the remaining junctions are formed by epitaxial growth. This particular design has reached efficiencies of approximately 41% under concentration. Further increases in efficiency have resulted from variations to the design such as using a metamorphic (not lattice matched) bottom sub-cell with a more optimal band gap.

As research in multi-junction cells continues to push towards higher efficiencies, increasingly sophisticated designs are being studied including 4, 5 and 6-junction structures, metamorphic (non-lattice matched) structures, and designs using 'difficult' materials such as dilute nitrides. There is also a trend toward smaller cells which can operate efficiently at higher concentrations.

In this study we review the fundamental operation of multi-junction solar cells and present a simple method for evaluating performance of proposed multi-junction designs before embarking on a more detailed analysis. We then discuss each of the approaches mentioned above, giving examples of possible designs. Finally we study cell efficiency for varying cell size, gridline spacing and gridline width as a function of concentration.

2. Multi-junction Solar Cells

With single-junction solar cells, two primary types of losses tend to limit efficiency: Thermalization (loss of photon energy greater than the band gap of the junction material) and non-absorption (inability to absorb photons with energy less than the band gap). When these are considered together with a third loss mechanism, emission of thermal photons, we arrive at the well-known Shockley-Queisser limit on single-junction cell solar efficiency [5]. The Shockley-Queisser analysis gives us a conservative upper limit on the potential efficiency of a single junction with a given band gap. If we optimize for a terrestrial application and take AM1.5D as the reference spectrum [6], the optimal band gap is 1.4 eV. In this optimal case, thermalization results in losses of 19.8% and non-absorption amounts to losses of 34.9%. These losses are independent of concentration. The (smaller) loss fraction due to thermal photon emission will decrease somewhat with increasing concentration, as will be discussed below.

To produce cells with efficiency exceeding the single-junction Shockley-Queisser limit, we stack multiple cells on top of one another with band gap decreasing from the top down. In this, way, photons which would be lost through non-absorption in the top sub-cell may be absorbed by a lower band-gap sub-cell (Figure 1). This arrangement also ensures that photons are absorbed by a sub-cell with band gap energy similar to the photon energy and so both non-absorption and thermalization losses are reduced. In theory, with ideal choices of materials and an infinite number of sub-cells the non-absorption and thermalization

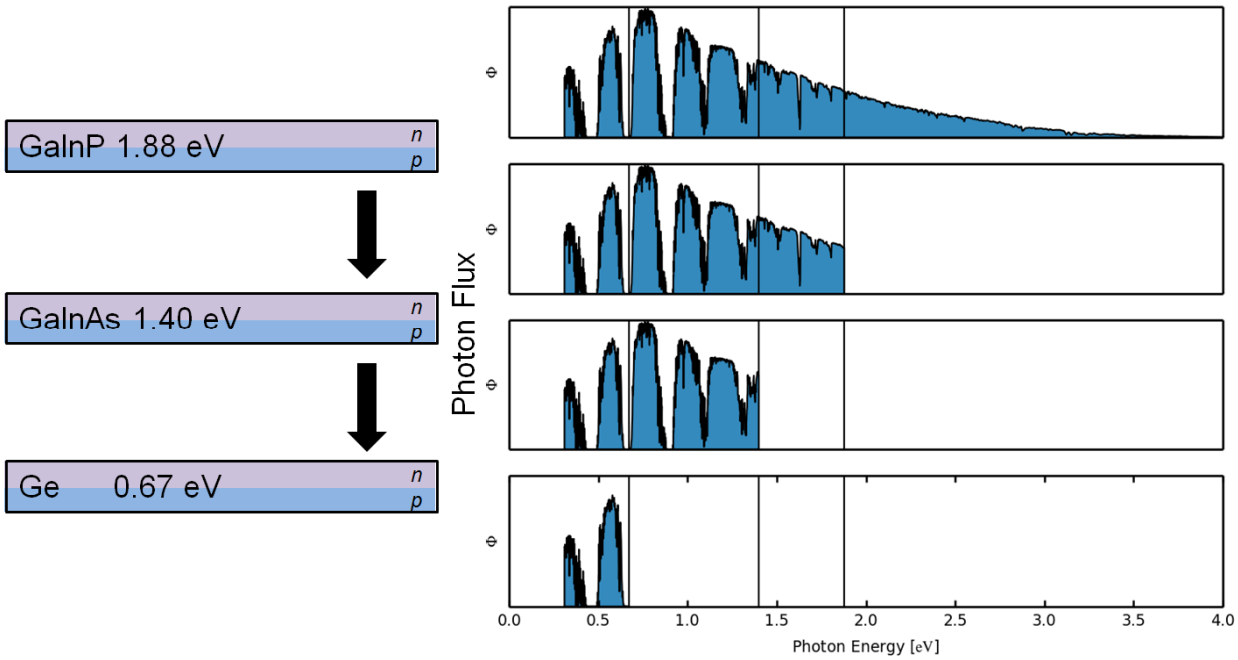

Figure 1: Each sub-cell absorbs the portion of the incident spectral photon flux with energy greater than its band gap.

losses could be eliminated completely, leaving only the thermal photon emission losses.

Typically, the layers of a multi-junction solar cell may be as shown in Figure 2 for a GaInP/Ga(In)As/Ge cell – though in practice there may be even more layers, such as diffusion barrier layers surrounding the tunnel junctions, 2-layer anti-reflection coatings (ARCs) and intrinsic or graded doping layers within the sub-cell junctions.

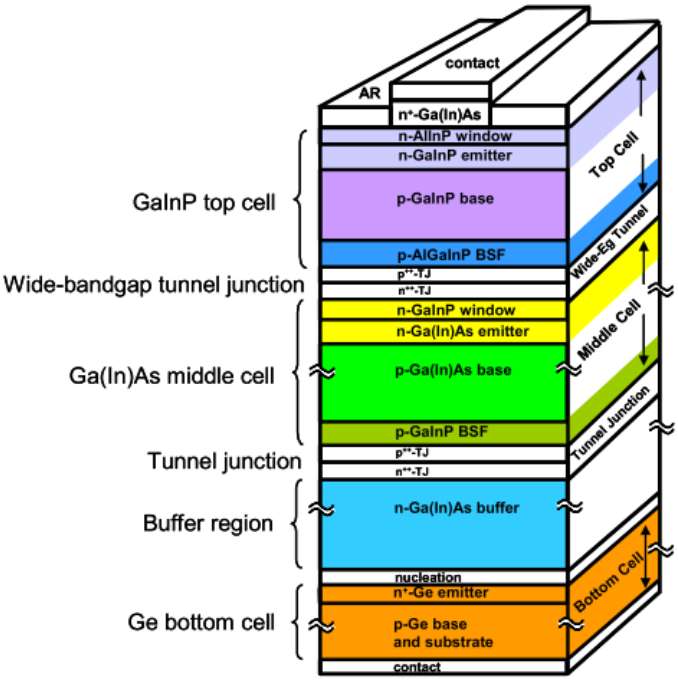

Figure 2: The layers of a 3-junction GaInP/Ga(In)As/Ge solar cell. From [21]**.**

A very simple equivalent circuit model for the triple-junction cell is shown in Figure 3, using a one-diode model to represent each of the sub-cells. Kirchoff's law requires that the total current at the terminals and the total current through each of the sub-cells is equal; since the diodes should have negligible reverse current, in order to have a positive current density J at the terminals we require positive photocurrent densities $J_{ph,i}$ in each of the sub-cells. Indeed, neglecting any reverse diode current or shunt conductivity in the limiting sub-cell, the 1-sun short-circuit current density is

$$J_{SC} = \min\left(J_{ph,i}\right). \tag{1}$$

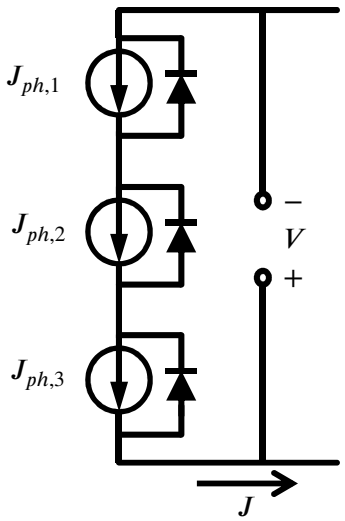

Figure 3: Simple equivalent circuit model for a three-junction *n-p* solar cell. Each junction is represented by a current source and diode.

This result implies that, in order to maximize J_{SC}, the available photon flux should be split equally between all sub-cells. This condition is called 'current matching'.

3. Approximate Analysis using Band Gap – Voltage Offset

As we will see below, when we allow for advanced techniques such as wafer bonding and metamorphic crystal growth, there are a myriad of possible cell structures that might be considered. Before embarking on detailed analysis of any particular structure – which may require considerable research to find appropriate material parameters and physical models – we should use a simpler analysis to evaluate the potential performance of various possible designs. The Shockley-Queisser analysis could be used for this purpose, but the resulting efficiencies are generally unachievable in practice. Richard King of Spectrolab has used an empirical model to very good effect [3, 7]. His model is based on the observation that experimentally measured single-junction solar cells of many different materials have a band gap-voltage offset $E_g/q - V_{OC} \cong 0.4$ V at 1 sun; this is illustrated in Figure 4. The very highest quality materials, such as GaAs as well as Ga(In)As grown lattice matched on a Ge substrate, have a band gap – voltage offset of

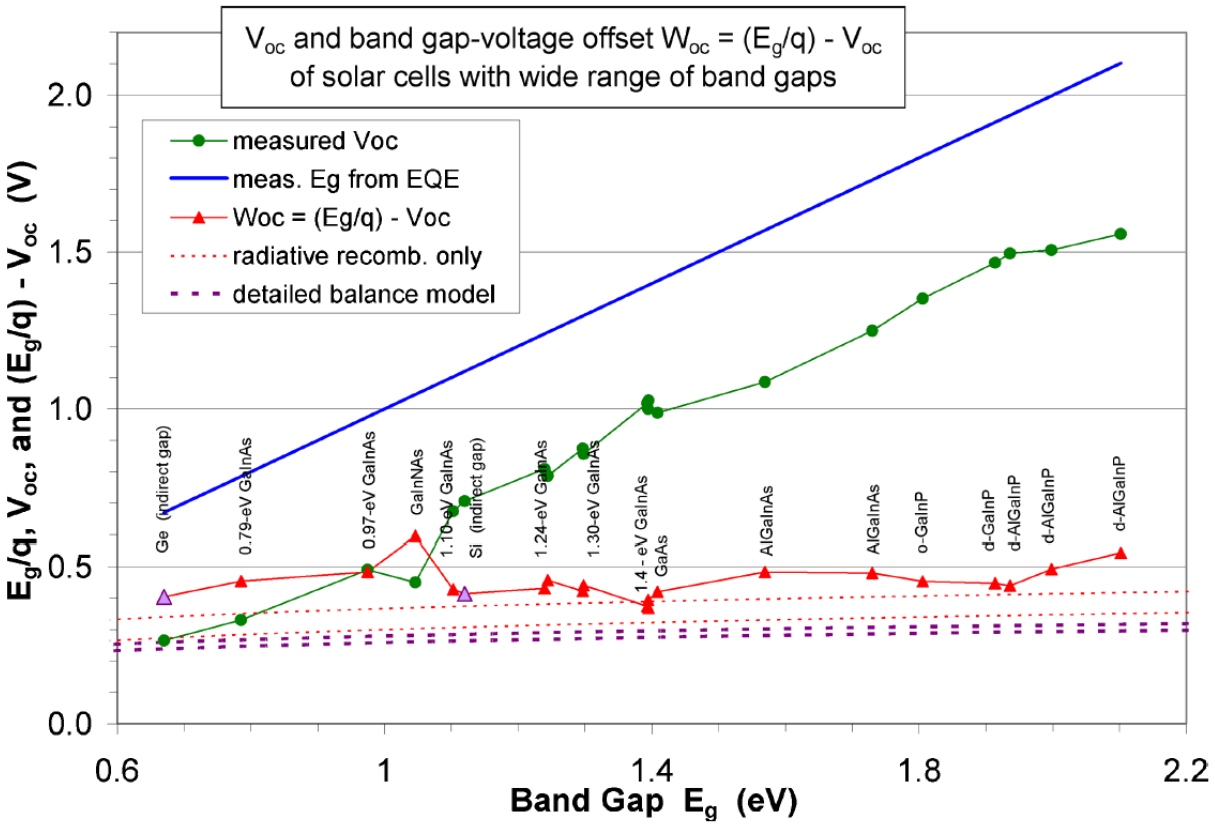

Figure 4: (green) 1-sun V_{OC} vs. band gap E_g for a variety of solar cells. (red) band gap-voltage offset $E_g - V_{OC}$ for the same cells. (red dashed lines) Calculated $E_g - V_{OC}$ based on radiative recombination. (purple dashes) $E_g - V_{OC}$ based on detailed balance analysis. From [3]**.**

0.4 V, while some disordered ternary and quaternary alloys have offsets up to 0.5 V. Dilute nitrides lattice matched to GaAs are shown with a band gap-voltage offset ~ 0.6V. Also shown in the figure are theoretical estimates of $E_g/q - V_{OC}$ based on detailed balance arguments, and based on an assumption that recombination is dominated by radiative recombination with no photon recycling.

Having estimated the 1-sun open-circuit voltage $V_{OC,i}$ for each of the sub-cells in a given design, we can then estimate $J_{ph,i}$ using the definition

$$J_{ph,i} = q \int_0^\infty \Phi(E) EQE_i(E) dE, \tag{2}$$

where $\Phi(E)$ is the photon flux density at energy E, and $EQE_i(E)$ is the external quantum efficiency of sub-cell i. For high-quality III-V devices, we can assume the best case and use the approximation

$$J_{ph,i} \cong q \int_{E_{g,i}}^{E_{g,i-1}} \Phi(E) dE. \tag{3}$$

Experimentally measured EQE of two different multi-junction cells, a III-V GaInP/Ga(In)As/InGaAs cell and a 2J organic cell, are shown in Figure 5. The approximation in (3) applies well to the III-V cell, with two caveats: (1) the EQE of the top cell is limited by the band gap of its front surface field, and (2) the figure is normalized (each sub-cell is scaled to peak at 100% EQE). Nonetheless, for a III-V cell optimized for 1-sun operation, EQE would be expected to peak very near 100%.

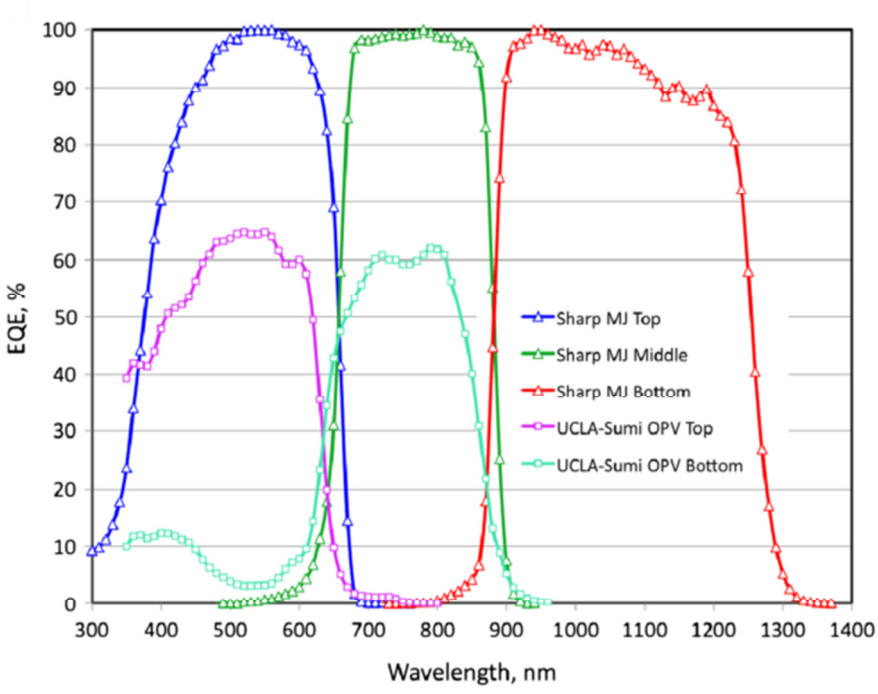

Figure 5: External quantum efficiency of a 3J GaInP/GaAs/InGaAs, 37.5% efficient at 1-sun solar cell from Sharp (normalized data) and a 2J, 10.6% efficient organic solar cell from UCLA/Sumitomo. From [23]**.**

Now, for 'well-behaved' sub-cells,

$$J_i = J_{ph,i} - J_{dark}(V_i). \tag{4}$$

At $V_i = V_{OC,i}$, $J_i = 0$ by definition and so

$$J_{ph,i} = J_{dark}\left(V_{OC,i}\right). \tag{5}$$

Assuming a single-diode dark current for each sub-cell,

$$J_{ph,i} = J_{0,i}\,[exp\left(\frac{qV_{OC,i}}{n_i kT}\right) - 1], \tag{6}$$

$$\text{and } J_{0,i} = \frac{J_{ph,i}}{\exp\left(\frac{qV_{OC,i}}{n_i kT}\right) - 1} \tag{7}$$

Where kT is the thermal voltage (~ 26mV at 300K), and n_i is the diode ideality factor. For a best-case analysis, the ideality factors can be assumed equal to 1. We can now write an expression for the $J_i - V_i$ relation in each sub-cell,

$$J_i(V) = X J_{ph,i} - J_{0,i}\left[\exp\left(\frac{qV_i}{n_i kT}\right) - 1\right], \tag{8}$$

where we include a concentration factor X to allow for changing optical intensity.

We can then find the full-device short-circuit current density from (1) and (8),

$$J_{SC} = X \min(J_{ph,i}), \tag{9}$$

and the full-device $V_{OC} = \sum_i V_{OC,i}$,

$$V_{OC} = \frac{kT}{q}\left[\sum_i n_i \ln\left(\frac{J_{ph,i}}{J_{0,i}}\right) + \ln X \sum_i n_i\right]. \tag{10}$$

The relation (10) is very interesting in that there are two terms, only one of which is dependent on concentration. We do not derive it here, but fill factor also increases with increasing concentration (neglecting effects of parasitic resistances). While it is generally preferable to have low ideality factors, (10) indicates that the V_{OC} of cells with higher ideality factors will respond more strongly to changes in concentration. Hence if the incident optical power is EX and the power production is$J_{SC}V_{OC}FF$, where E is the one-sun optical intensity and FF is the solar cell fill factor, then neglecting the dependence of fill factor on X we can find the variation of efficiency with concentration,

$$\frac{d\eta}{dX} \cong FF\,\frac{d}{dX}\left(\frac{X \min(J_{ph,i})\frac{kT}{q}\left[\sum_i n_i \ln\left(\frac{J_{ph,i}}{J_{0,i}}\right) + \ln X \sum_i n_i\right]}{EX}\right) \tag{11}$$

$$\frac{d\eta}{dX} \cong \frac{FF \cdot kT}{qE}\frac{d}{dX}\left(\min(J_{ph,i})\left[\sum_i n_i \ln\left(\frac{J_{ph,i}}{J_{0,i}}\right) + \ln X \sum_i n_i\right]\right) \tag{12}$$

$$\frac{d\eta}{dX} \cong \frac{FF \cdot kT}{qE} \min(J_{ph,i}) \frac{d}{dX}(\ln X) \sum_i n_i \tag{13}$$

$$\frac{d\eta}{dX} \cong \frac{1}{X} \frac{FF \cdot kT}{qE} \min(J_{ph,i}) \sum_i n_i. \tag{14}$$

We should note that the analysis as presented here only holds for relatively low intensities; in order to consider higher intensities we must include some additional parasitic effects. These effects, particularly series resistances, generally determine the peak in efficiency vs. concentration.

4. Grid Optimization and Cell Size

Some of the parasitic effects that we should consider are illustrated in Figure 6. They are (1) series resistance due to lateral conduction through the emitter of the top sub-cell, (2) contact resistance at the grid finger/semiconductor interface, (3) conduction along the grid fingers, (4) shadowing of the cell by the grid fingers, (5) uneven bias across the cell due to resistive voltage drops, (6) perimeter recombination (surface recombination occurring at the exposed perimeter surfaces of the solar cell), and (7) shunt conductance. The shadowing can be modeled very easily by reducing the photo-generated currents $J_{ph,i}$ proportionate with the fraction of shaded cell. The resistances can be modeled by adding lumped series

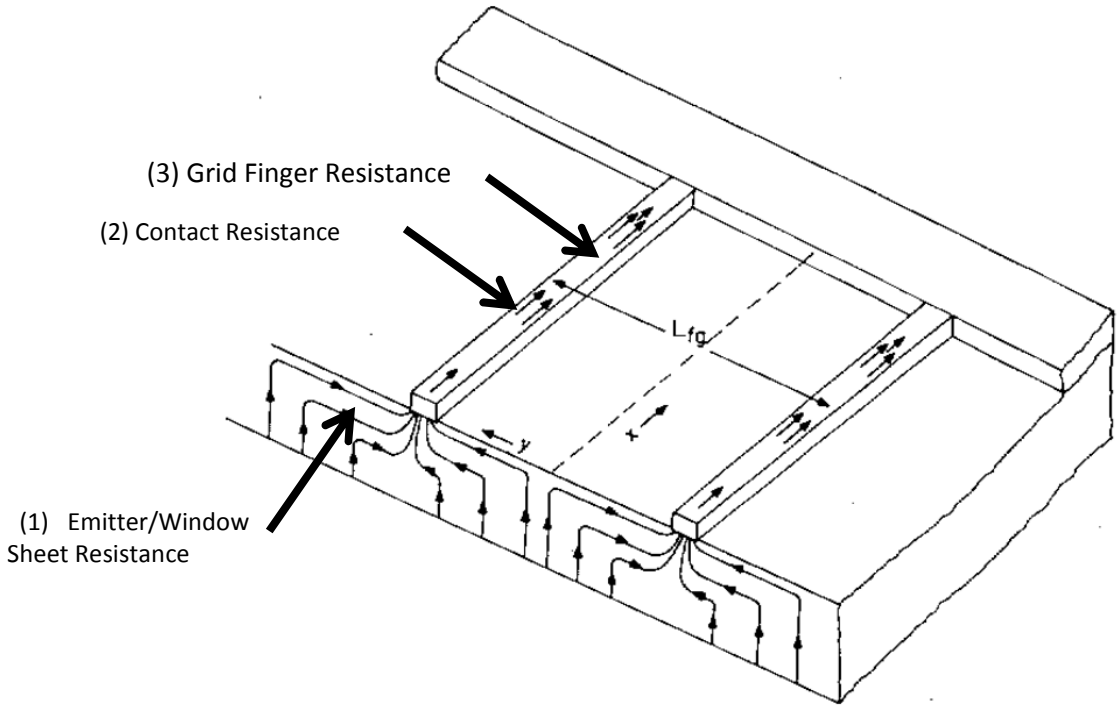

Figure 6: Parasitic resistances due to the top contact grid. Figure from [8]**.**

resistances to the equivalent circuit model in Figure 3, with resistance values calculated as described in the references [8, 9], so that the total power dissipation in the resistive elements is equal to the total losses for each mechanism. Shunt conductance should be negligible in high-quality III-V materials, but may be significant if there are processing defects.

The remaining mechanisms – perimeter recombination and uneven bias (sometimes called 'non-generation losses') – require a more sophisticated model such as a drift-diffusion model or a distributed lumped-parameter model. Perimeter recombination may be significant for 10 mm x 10 mm device sizes (as was 'tentatively' suggested for the 1 cm^2 5J cell in [10]), but becomes increasingly important for smaller devices where the perimeter-to-area ratio is larger [11, 12].

As an example, we'll consider two designs, a 3J lattice-matched GaInP/GaInAs/Ge cell and a 4J AlGaInP/GaAs/InGaAs/InGaAs design which requires two metamorphic buffers. Parameters are as follows:

	3J GaInP/GaAs/Ge	**4J AlGaInP/GaAs/InGaAs/InGaAs**
Sub-cell 1	GaInP (1.85 eV)	AlGaInP (1.85 eV)
Sub-cell 2	Ga(In)As (1.40 eV)	AlGaAs (1.48 eV)
Sub-cell 3	Ge (0.67 eV)	InGaAs (1.12 eV)
Sub-cell 4	n/a	InGaAs (0.75 eV)
$\boldsymbol{\rho_s}$	300 Ω/□	300 Ω/□
$\boldsymbol{\rho_m}$	$10^{-5}\Omega \cdot \mathrm{cm}$	$10^{-5}\Omega \cdot \mathrm{cm}$
$\boldsymbol{\rho_c}$	$4 \times 10^{-5}\Omega \cdot \mathrm{cm}^2$	$4 \times 10^{-5}\Omega \cdot \mathrm{cm}^2$
$\boldsymbol{n}$	4	4

ρ_s is the emitter sheet resistance, ρ_m is the gridline metal resistivity, and ρ_c is the contact resistivity of the metal/semiconductor interface. n is the ratio of gridline height to width. A sample of the resulting sub-cell and full-device $J - V$ curves is shown in Figure 7 for 1-sun, AM1.5D conditions, with series resistance and grid shading neglected. It is apparent that the Ge sub-cell in the classic 3J design has excessive photocurrent compared with the other sub-cells. While this slightly increases V_{OC} and FF of the cell, the available photon flux could be better used with a larger band gap in the bottom junction. Alternatively, as in the 4J design, the bottom sub-cell photocurrent can be split between two sub-cells, providing a significantly increased operating voltage. Theoretical 1-sun efficiencies for the 3- and 4-junction devices are 34.8% and 42.2%, respectively.

When we include shading and resitance, and vary the grid finger width and spacing over a range of values, we can determine an optimal grid design for any given concentration. Figure 8 and Figure 9

show the results of such an optimization study for the 4J cell, with 1 cm^2 (10 mm × 10 mm) and 0.04 cm^2 (2 mm × 2 mm) aperture sizes. Clearly the optimal grid parameters are dependent on the intended concentration, but fortunately in most cases there is a wide 'plateau' surrounding the optimal design point so performance will not be overly sensitive to the chosen design.

The results of the optimization study are more concisely represented in Figure 10 (a), where it is clear that the 0.04 cm^2 cell reaches a higher peak efficiency, and at a higher concentration. This is because current has a shorter lateral distance to travel to reach the busbars at the edge of the cell, and so the fraction of resistive losses is lower at a given current density. It is likely that at this cell size perimeter recombination is also significant and would shift the point of peak efficiency to lower values if it were included in the simulation.

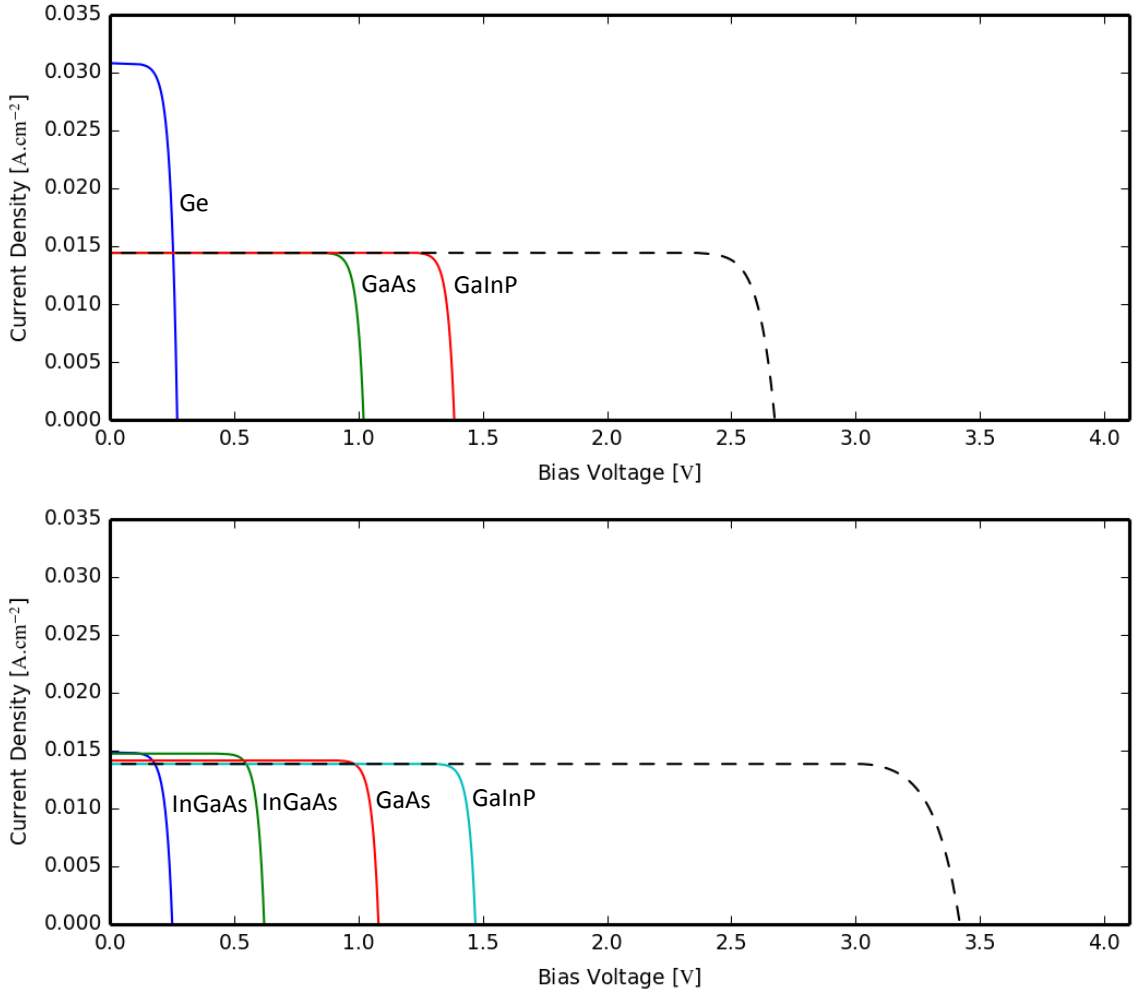

Figure 7: Estimated sub-cell (solid) and full device (dashed) $J - V$ curves under 1-sun (1000 W/m^2), AM1.5D conditions for (a) a 3J GaInP/GaAs/Ge solar cell and (b) a 4J GaInP/GaAs/InGaAs/InGaAs with two metamorphic buffer layers.

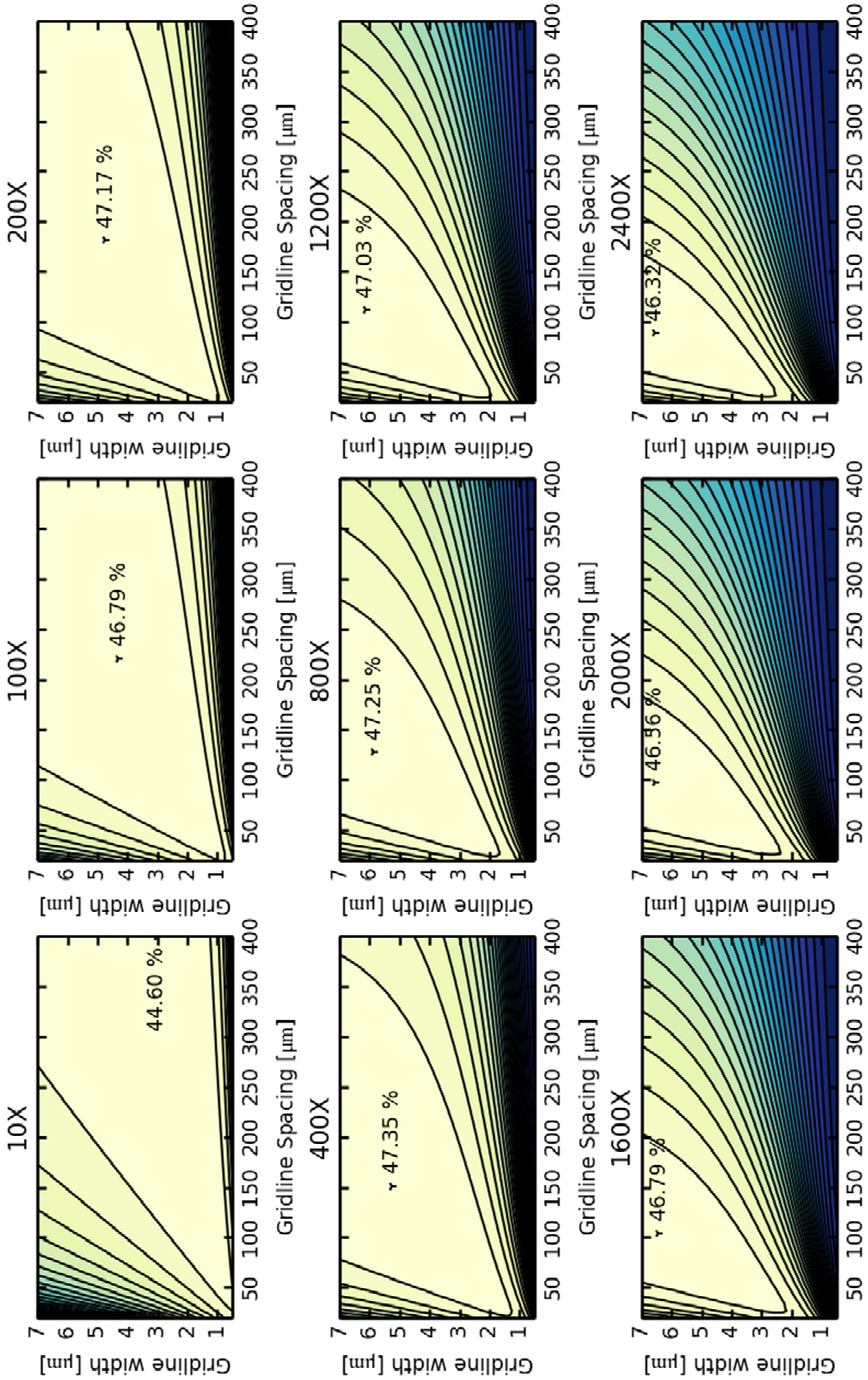

Figure 8: Efficiency of 10 mm x 10 mm, 4-junction solar cell with two metamorphic buffers as a function of concentration factor *X* and grid design parameters. The optimum grid design and corresponding efficiency is marked for each concentration.

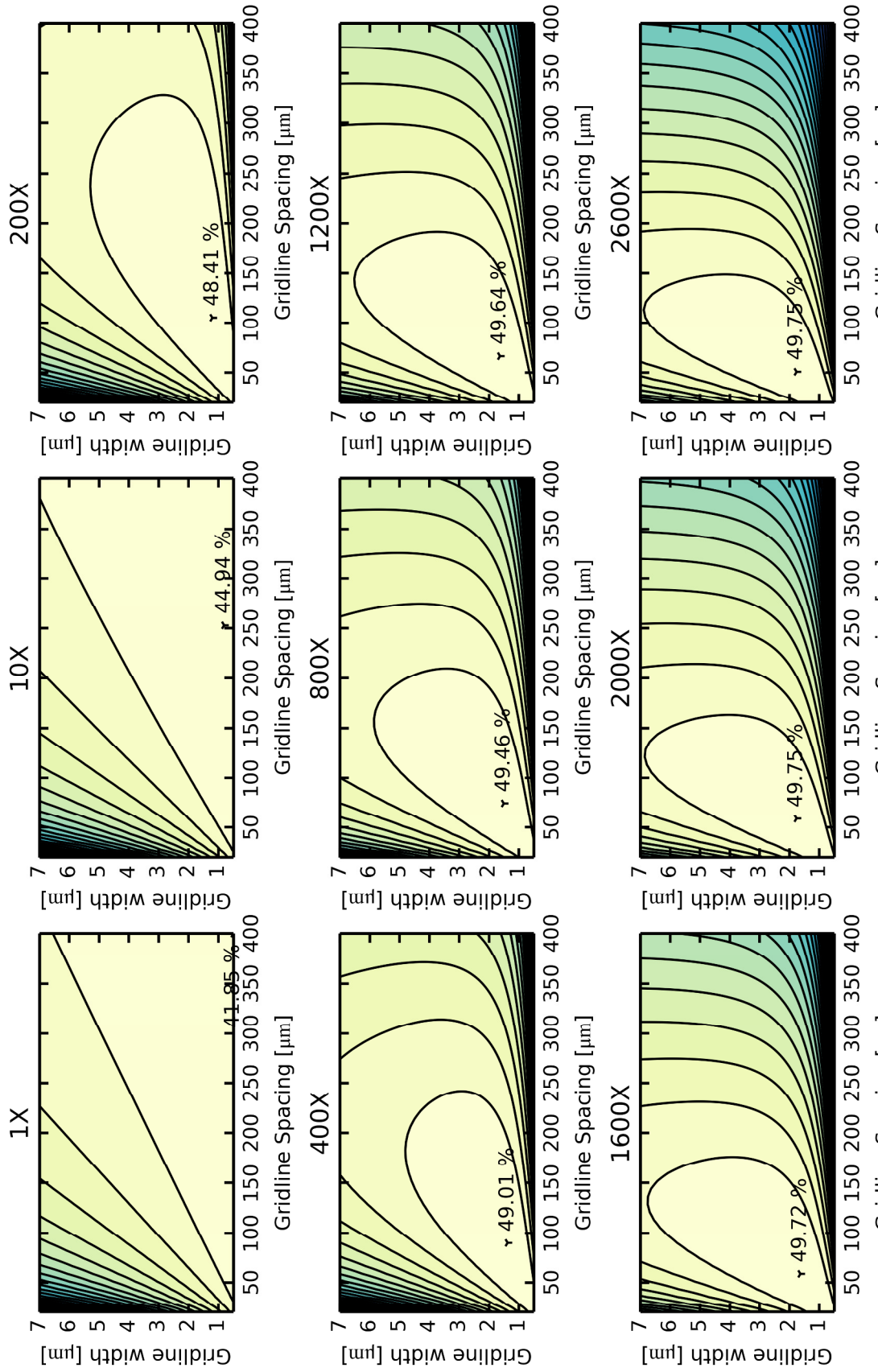

Figure 9: Efficiency of 2 mm x 2 mm, 4-junction solar cell with two metamorphic buffers as a function of concentration factor *X* and grid design parameters. The optimum grid design and corresponding efficiency is marked for each concentration.

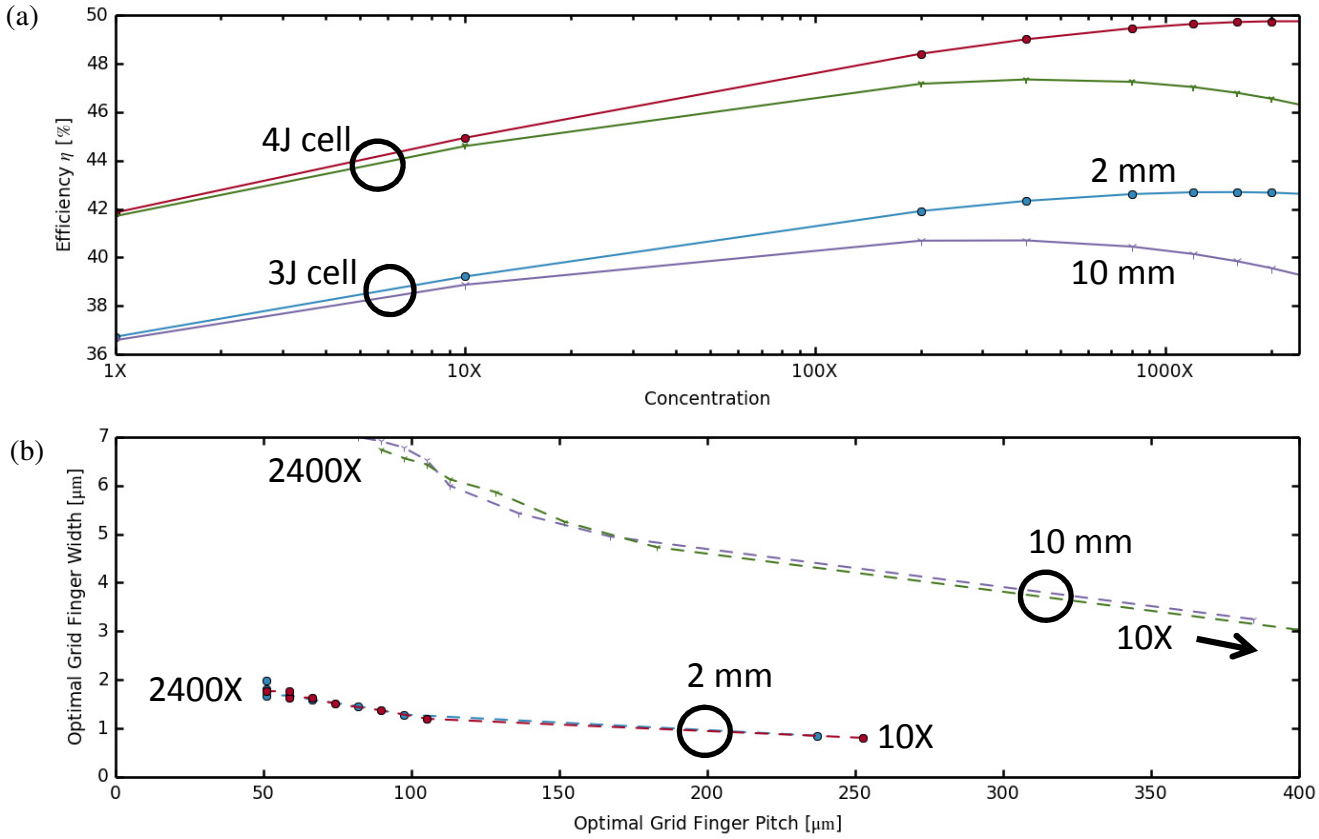

Figure 10: (a) Efficiency of 3J and 4J cells vs. concentration, for 2 mm x 2mm and 10 mm x 10 mm cell sizes. Grid dimensions are optimized individually for each data point. (b) Optimal grid designs at each concentration.

We see a roughly 3% (absolute) increase in efficiency for the 0.04 cm^2 compared with the 1 cm^2 cell, and the concentration at peak efficiency is increased by a factor of 5. In Figure 10 (b), the changes in optimal grid design are plotted. In general, increasing concentration requires wider and more closely-spaced gridlines, as might be expected.

The set of solutions for the 3J cell and for the 4J cell lie alomost directly on top of one another, but at a given concentration the 4J cell takes slightly smaller gridlines as a result if its lower ratio of maximum-power current density to voltage, J_m/V_m. Optimal grids for the 0.04 cm^2 cells have much narrower grid fingers than for the 1 cm^2 cells. In general, increasing the number of junctions not only accomplishes the primary goal of reducing thermalization and non-absorption losses, but also carries benefits in reducing resistive and shading losses.

5. Design Approaches

5.1. Lattice Matched Designs

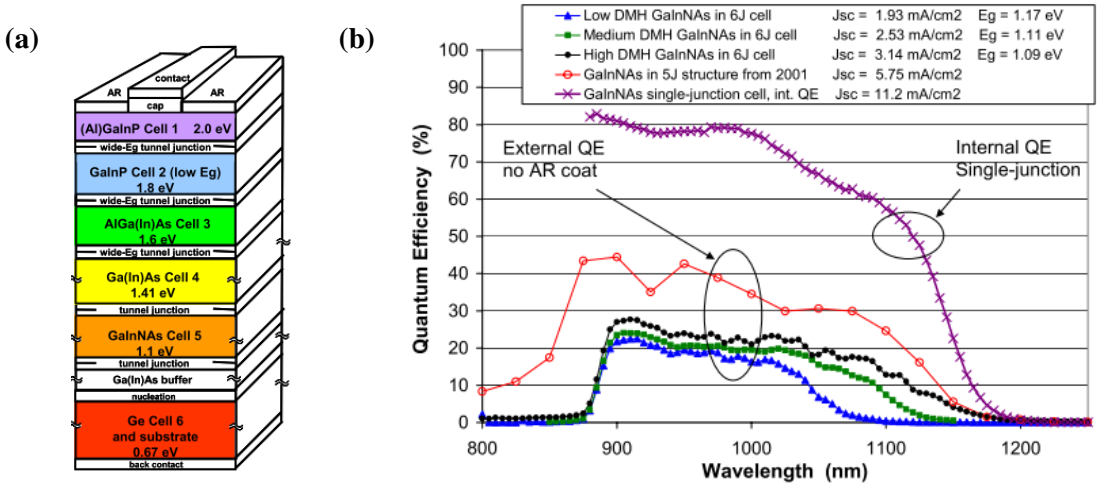

Figure 11: (a) Spectrolab's 6-junction lattice matched solar cell structure with GaInNAs sub-cell. From [21]**. (b) Quantum efficiency of ~1.1 eV dilute nitride junctions in a 6-junction solar cell, grown lattice matched to Ge. From** [21]**.**

In order to improve on the classic GaInP/GaAs/Ge 3J design in a lattice-matched configuration, we need a ~1.0 eV material with Zincblende crystal structure, lattice matched to Ge or GaAs, which can either replace the Ge sub-cell or be added above it. One of the only such materials is the dilute nitrides such as GaInNAs. These have been demonstrated most successfully by Solar Junction with their record 43.5% and 44.0% efficient GaInP/GaAs/GaInNAs concentrator cells [13].

Previously, Spectrolab and NREL had pursued designs with as many as 6 junctions including dilute nitrides, as illustrated in Figure 11. The 6-junction experiment was severely limited by the low photocurrent in the dilute nitride sub-cell. Dilute nitrides have extremely short diffusion lengths, requiring *p-i-n* structured cells. They are generally lossy, with low quantum efficiency, a large bandgap-voltage offset (0.6V in Figure 4), and poor fill factor due to their *p-i-n* structure. Thus the material does not fit well in highly engineered many-junction designs which are intended to eliminate losses wherever possible.

5.2. Metamorphic Designs

The National Renewable Energy Lab (NREL) has developed a process for 3J 'inverted metamorphic' (IMM) solar cells where the top two junctions are grown lattice matched, 'upside down' on a GaAs wafer, followed by a metamorphic buffer layer and an InGaAs junction with different lattice constant (Figure 12). The structure is then bonded to a 'handle' – such as a glass slide – and removed from the GaAs wafer by etching away a sacrificial layer of AlGaAs.

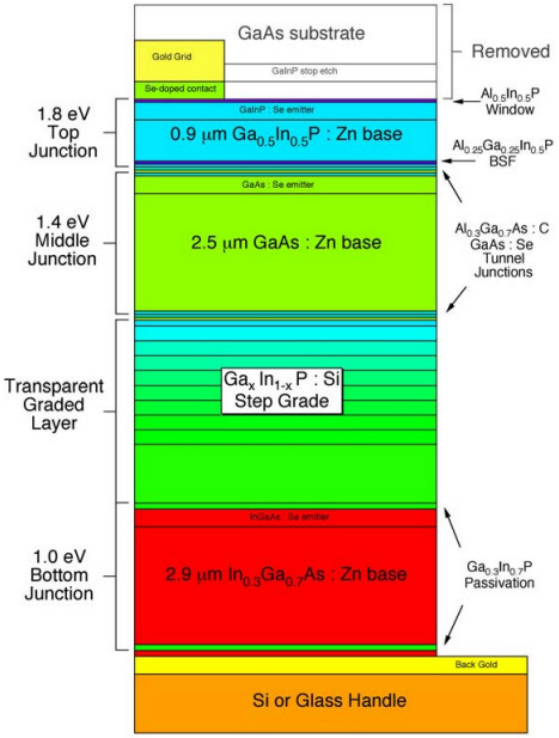

Figure 12: Structure of NREL's 3J inverted metamorphic (IMM) solar cell. From [22]**.**

This process has been licensed by Emcore for use in space cells; several record concentrator cells have also been made in recent years using the metamorphic approach. The concept can be extended further with multiple junctions below the graded layer, or by including multiple grades to achieve great flexibility. NREL was able to refine the growth of the step-graded metamorphic buffer such that the InGaAs material grown on top of it was under minimal stress [14]. This yielded high quality InGaAs with dislocations in the low 10^6 cm^{-2} range and sub-cell band gap-voltage offsets of less than 0.5 V.

5.3. Wafer Bonded Designs

Another approach which has shown remarkable success in recent years is wafer bonding, where groups of subcells are grown on two different wafers of different lattice constants (GaAs and InP) which are then bonded together. In some cases the 'bonding' is simply a matter of polishing cleaning or otherwise 'activating' the surfaces and touching them together; the clean crystal surfaces naturally adhere to one another [15].

In 2013, Spectrolab demonstrated a 5-junction device of this type in both 1 cm^2 concentrator form and as 20 cm^2, 1-sun space cells [10]. The EQE, IQE and reflectance of the space cell are shown in Figure 14, and an infrared electroluminescence image is in Figure 14. The even illumination indicates a minimum of voids in the wafer bonding process, and interestingly, the 20 cm^2 cells had slightly higher V_{OC} and efficiency, which was 'tentatively attributed' to reduced perimeter recombination in the large cell.

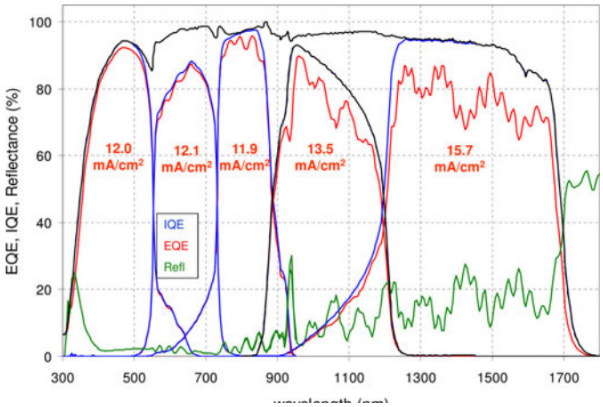

Figure 14: (red) sub-cell EQE, (blue) IQE and (green) reflectance of a 5J wafer-bonded cell. Sub-cell short-circuit currents are also shown, with a correction for busbar losses. From [10]**.**

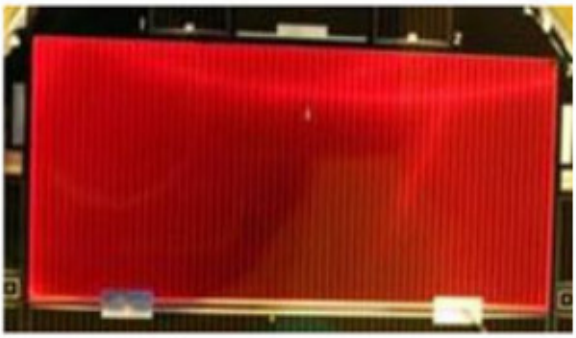

Figure 14: Forward-biased infrared (FBIR) image of a 20 cm^2, 5J wafer-bonded solar cell from Spectrolab. From [10]**.**

Spectrolab did note that the cell had a specific resistance of 2 $\Omega \cdot \text{cm}^2$ which was likely due to the bond, and which caused the cell to peak in efficiency at only 10 X concentration. Another example of wafer bonding is the current world record, four-junction, 44.7% efficient cell made by Soitec in collaboration with Fraunhofer ISE. The peak efficiency was measured on a 5.2 mm^2 cell at 297 suns [16].

6. Wide Band Gap Tunnel Diodes

In order to minimize losses in the tunnel diodes of multi-junction cells, it is important that the layers the tunnel junction are made of materials with band gap no smaller that the cell above it; otherwise some photons would be absorbed in the tunnel junction rather than being transmitted into the next sub-cell. While GaAs and AlGaAs/GaAs tunnel junctions are widely used in practice, and GaInP/AlGaAs tunnel junctions have also been used successfully, this constraint becomes a challenge for designs with very large-band gap sub-cells (> 2.0 eV for example). A large band gap generally implies a very strong attenuation of wave functions tunneling through the middle of the gap; the peak tunneling current for a tunnel junction varies with the tunneling probability which is, to first order, given by

$$T \cong \exp\left(-\frac{4\sqrt{2m^*}E_g^{3/2}}{3q\hbar\mathscr{E}}\right), \tag{15}$$

where m^* is effective mass, $\hbar$ is the reduced Planck's constant, q is electron charge, and $\mathscr{E}$ is the electric field strength in the junction [17]. Additionally, it can be challenging to achieve degenerate doping in large band gap materials. Combined, these factors make it difficult to produce usable tunnel junctions (i.e. tunnel junctions with a tunneling peak current density greater than the short-circuit current density of a concentrator cell) from wide band gap materials. In some cases a heterojunction, such as

AlGaAs/GaAs, can provide a favorable band offset and reduce the level of doping required to produce degeneracy on both sides of the junction [18]. More recently, some researchers have used quantum wells within the tunnel junctions to enhance tunneling current density [19, 20].

7. Conclusions

There is a vast array of possible approaches to next-generation multi-junction solar cells within the III-V material system. Increasing numbers of junctions are sure to be a theme for the next several years, as it helps to reduce thermalization and non-absorption losses, and has secondary benefits with reduced resistive and shadowing losses. Commercial demand for CPV cells is trending toward smaller cell sizes, from 1 cm^2 a few years ago to 0.25 cm^2 to 0.05 cm^2 today. The smaller cell sizes have lower series resistance and are more suited to higher concentrations and smaller optical systems.

Wafer bonding is inherently expensive as it requires multiple growths on different substrates, but the results achieved with it to date are very promising. Soitec and Spectrolab are both working on developing it as a commercially viable technology for the CPV market. Metamorphic growth gives even more flexibility in material choices, since there can be multiple graded buffer regions within a structure. It seems that the ability to make these structures is primarily limited by the availability of a single reactor capable of growing a sufficiently wide range of materials and dopants. Both wafer bonds and metamorphic buffers can potentially introduce series resistance, but it is not clear if this is limiting performance of the best cells in the literature. Dilute nitride-based designs are also interesting, but the material quality will have to advance significantly to make these sub-cells competitive with non-lattice-matched 1.0 eV options such as InGaAs.

References

[1] M. A. Green, K. Emery, Y. Hishikawa, W. Warta, and E. D. Dunlop, "Solar cell effi ciency tables (version 43)," *Prog. Photovoltaics Res. Appl.* **22**, pp. 1–9, 2014.

[2] "Best Research-Cell Efficiencies," *National Renewable Energy Laboratory Website*, 2012. [Online]. Available: http://www.nrel.gov/ncpv/images/efficiency_chart.jpg. [Accessed: 08-Jan-2013].

[3] R. R. King, D. Bhusari, D. Larrabee, X. Liu, E. Rehder, K. Edmondson, H. Cotal, R. K. Jones, J. H. Ermer, C. M. Fetzer, D. C. Law, and N. H. Karam, "Solar cell generations over 40 % efficiency," *Prog. Photovoltaics Res. Appl.* **20**, pp. 801–815, 2012.

[4] Z. S. Judkins, "A Market Analysis for High-Efficiency Multi-Junction Solar Cells Grown on SiGe," Thesis, Department of Materials Science and Engineering, MIT, 2007.

[5] W. Shockley and H. J. Queisser, "Detailed Balance Limit of Efficiency of p-n Junction Solar Cells," *J. Appl. Phys.* **32** (3), p. 510, 1961.

[6] "ASTM G173-03 (2008) Standard Tables for Reference Solar Spectral Irradiances: Direct Normal and Hemispherical on 37 degree Tilted Surface," 2008.

[7] R. R. King, D. Bhusari, A. Boca, D. Larrabee, X. Liu, W. Hong, C. M. Fetzer, D. C. Law, and N. H. Karam, "Band gap-voltage offset and energy production in next-generation multijunction solar cells," *Prog. Photovoltaics Res. Appl.* **19**, pp. 797–812, 2011.

[8] A. R. Moore, "An Optimized Grid Design for a Sun-Concentrator Solar Cell," *RCA Rev.* **40**, pp. 140–152, 1979.

[9] T. A. Gessert and T. J. Coutts, "Grid metallization and antireflection coating optimization for concentrator and one-sun photovoltaic solar cells," *J. Vac. Sci. Technol. A* **10** (4), p. 2013, Jul. 1992.

[10] P. T. Chiu, D. C. Law, R. L. Woo, S. B. Singer, D. Bhusari, W. D. Hong, a. Zakaria, J. Boisvert, S. Mesropian, R. R. King, and N. H. Karam, "Direct Semiconductor Bonded 5J Cell for Space and Terrestrial Applications," *IEEE J. Photovoltaics* **4** (1), pp. 493–497, Jan. 2014.

[11] T. B. Stellwag, P. E. Dodd, M. S. Carpenter, M. S. Lundstrom, R. F. Pierret, M. R. Melloch, E. Yablonovitch, and T. J. Gmitter, "Effects of perimeter recombination on GaAs-based solar cells," in *Photovoltaic Specialists Conference 1990, IEEE 21st*, 1990, (100), pp. 442–447.

[12] O. Fidaner and M. Wiemer, "Power Output of Multijunction Solar Cell Wafers," in *CS MANTECH Conference*, 2013, (408), pp. 439–442.

[13] M. Wiemer, V. Sabnis, and H. Yuen, "43.5% Efficient Lattice Matched Solar Cells," in *High and Low Concentrator Systems for Solar Electric Applications VI*, 2011, **8108**, pp. 810804–1.

[14] A. Levander and J. Geisz, "EXAMINATION OF DISLOCATIONS IN LATTICE-MISMATCHED GaInAs/Buffer Layer/GaAs for III-V Photovoltaics," *U.S. Dep. Energy J. Undergrad. Res.*, pp. 55–62, 2005.

[15] K. Derendorf, S. Essig, E. Oliva, V. Klinger, T. Roesener, S. P. Philipps, J. Benick, M. Hermle, M. Schachtner, G. Siefer, W. Jager, and F. Dimroth, "Fabrication of GaInP/GaAs//Si Solar Cells by Surface Activated Direct Wafer Bonding," *IEEE J. Photovoltaics* **3** (4), pp. 1423–1428, Oct. 2013.

[16] "Soitec - World Record Solar Cell with 44.7% Efiiciency," 2013. [Online]. Available: http://www.soitec.com/en/news/press-releases/world-record-solar-cell-1373/. [Accessed: 02-Apr-2014].

[17] S. M. Sze and K. N. Kwok, *Physics of Semiconductor Devices*, 3rd ed. Hoboken, NJ: Wiley-Interscience, 2007, p. 832.

[18] J. F. Wheeldon, C. E. Valdivia, A. W. Walker, G. Kolhatkar, A. Jaouad, A. Turala, B. Riel, D. Masson, N. Puetz, S. Fafard, R. Ares, V. Aimez, T. J. Hall, and K. Hinzer, "Performance comparison of AlGaAs , GaAs and InGaP tunnel junctions for concentrated multijunction solar cells," *Prog. Photovoltaics Res. Appl.* **19** (4), pp. 442–452, 2010.

[19] U. Aeberhard, "Rigorous simulation of InAlGaAs-InGaAs bulk and quantum well interband tunnel junctions for multi-junction solar cells," in *2013 IEEE 39th Photovoltaic Specialists Conference (PVSC)*, 2013, (5), pp. 0154–0157.

[20] M. P. Lumb, M. K. Yakes, M. González, I. Vurgaftman, C. G. Bailey, R. Hoheisel, and R. J. Walters, "Double quantum-well tunnel junctions with high peak tunnel currents and low absorption for InP multi-junction solar cells," *Appl. Phys. Lett.* **100** (21), p. 213907, 2012.

[21] R. R. King, C. M. Fetzer, K. M. Edmondson, D. C. Law, P. C. Colter, H. L. Cotal, R. A. Sherif, H. Yoon, T. Isshiki, D. D. Krut, G. S. Kinsey, J. H. Ermer, S. Kurtz, T. Moriarty, J. Kiehl, K. Emery, W. K. Metzger, R. K. Ahrenkiel, and N. H. Karam, "Metamorphic III-V Materials, Sublattice Disorder, and Multijunction Solar Cell Approaches with over 37% Efficiency," in *19th European Photovoltaic Solar Energy Conference and Exhibition*, 2004, (June).

[22] J. F. Geisz, S. R. Kurtz, M. W. Wanlass, J. S. Ward, A. Duda, D. J. Friedman, J. M. Olson, W. E. Mcmahon, C. M. Kramer, M. S. Young, A. E. Kibbler, J. J. Carapella, P. Ahrenkiel, T. E. Moriarty, J. T. Kiehl, and K. E. Emery, "High Efficiency Inverted Monolithic Tandem GaInP / GaAs / InGaAs Solar Cells," pp. 3–4.

[23] M. A. Green, K. Emery, Y. Hishikawa, W. Warta, and E. D. Dunlop, "Solar cell efficiency tables (version 40)," *Prog. Photovoltaics Res. Appl.* **20**, pp. 606–614, 2012.